Solidification Morphology Analysis of SLM of Cu Powder

Jorge A. Ramos Grez
Pontificia Universidad Católica de Chile
Mechanical and Metallurgical Engineering Department

David L. Bourell
The University of Texas at Austin
Mechanical Engineering Department

ABSTRACT

The solidification morphology analysis of fine Cu powder melted by a raster scanned energy beam from a focused Nd:YAG laser is presented here. The powder was processed inside of sealed chamber where it was subjected to a high vacuum cycle. The laser fusion process consisted raster scanning a narrow rectangular pattern with a high density of scanning lines, the chamber was purged with inert gas during the process. Up to a 3.3 mm/s laser travel speed and maximum laser power level of 240 W were used to melt a 2 mm thick bed of loose powder. The resulting solidified ingots were separated into categories based on their shape integrity. Metallographic analysis by means of optical microscopy and scanning electron microscopy was performed on the cross section and longitudinal section of the ingots with homogeneous surface and complete shape integrity. Characterization revealed an elongated columnar grain structure with a grain orientation along the direction of the laser travel direction, some degree of porosity was observed too in some of the specimens. It was observed that grains diameter ranged from 10 to 100 μm and contained a two phase eutectic microstructure of copper and it oxides. Oxygen content was accounted from a 5.5 up to 8.1 atomic percent, a small percentage of chlorine was present, too. A 2 to 8 percent variation in the Vickers microhardness values were found between the different specimens when measured along the longitudinal section. These HV values corresponded to approximate 20-25% cold rolled oxygen free copper (80-90 HV). The ingots thus produced suggest that a multilayer structure from Cu powder could be build by the SLM process having sufficiently adequate compositional, microstructure and mechanical properties for functional applications.

INTRODUCTION

Selective laser melting (SLM) was developed during the 90s by the inventors of the SLS process [1,2]. In both processes a high power laser is raster scanned over the surface of a powder bed through a set of scanning mirrors. The powder material is kept at a temperature below the melting point of the alloy and is subjected to some kind of atmosphere. The laser beam provides the energy necessary to initiate sintering or fusion of the powder where laser beam is shine. The SLM process is aimed towards making functional metallic parts having high density and complex shapes starting off from loose metal powder [3,4]. Bonding of the metal particles is achieved through sintering under vacuum or at a pressure near to the atmospheric. In other cases, partial fusion of the powder is attained and thus a liquid phase sintering takes place. If the process is carried out over a thin layer of loose or mechanically compacted powder the result is a solid layer of reduced thickness having high densification. Complex shapes can be obtained when the beam is raster scanned over the surface of the powder bed [1,2].

Previous work done of direct laser sintering of Cu has been reported by Zhu *et al* [5]. Ramos and Bourell in recent collaboration with Japanese investigators have produced Ti-Ni shape memory alloy cast parts by the SLM process with successful results regarding the SM effect [6]. In this work the SLM method was applied to micron size Cu powder with the objective to understand better the type of macro and microstructure obtained, the degree of oxygen contamination, the densification achieved and the mechanical properties achieved.

EXPERIMENTAL PROCEDURE

Selective laser melting of single-layer Cu deposits was explored using the Nd:YAG laser based processing apparatus located at the Department of Mechanical Engineering of the University of Texas at Austin [7]. This workstation is shown in Figure 1 and it consists of a processing chamber that can reach vacuum levels of 10^{-6} Torr by means of a mechanical pump and a diffusion pump. Gas can be purged inside the chamber to provide specific atmospheric control. The laser power level and the motion of the galvanometer scanning mirrors are controlled by a personal computer through a DAQ

board (National Instruments). The laser head (U.S. Lasers) can generate up to 250 W in continuous wave mode. The optical system consists of a beam expander-collimator, a fused silica convex focusing length, galvanometer driven mirrors and a fused silica window. A beam spot of approximately 0.25 mm +/-0.05 mm can be obtained. The maximum power density of this system corresponds to $5.1*10^{-5}$ W/cm^2.

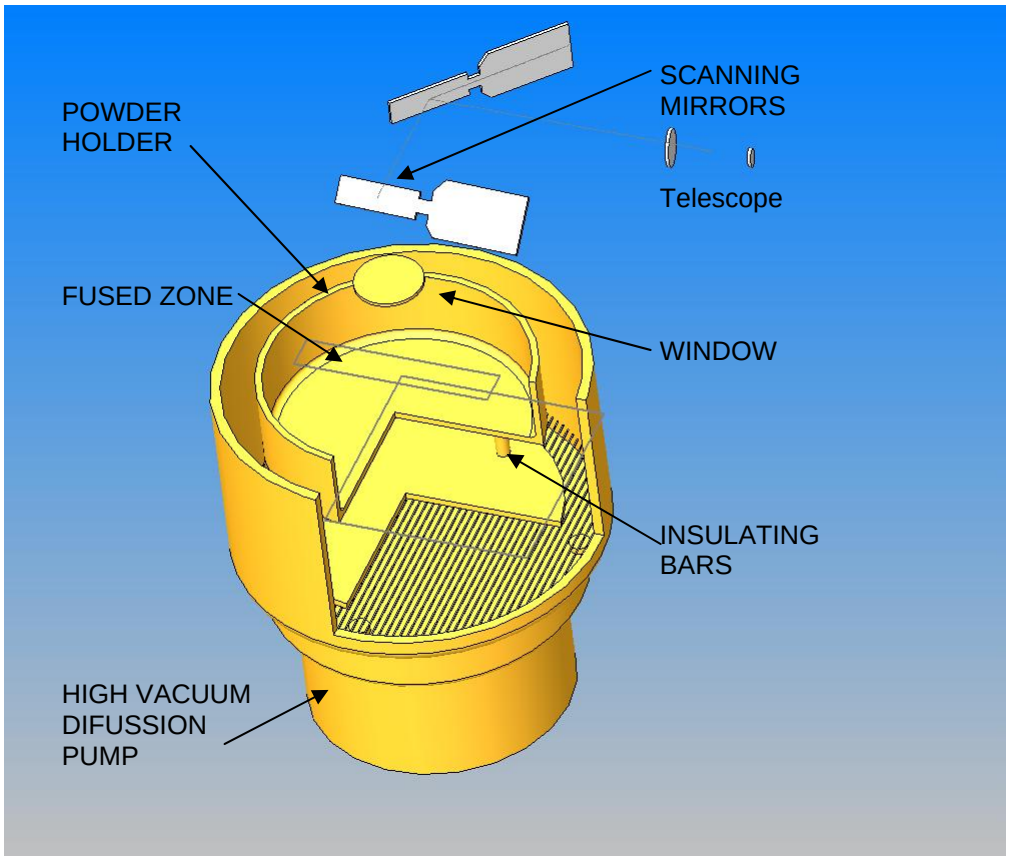

Figure 1. Schematic diagram of the SLM system employed.

The Cu powder was processed inside the sealed chamber in which it was subjected to high vacuum cycle and then purged with Ar gas. The laser raster scanning process consisted of a narrow rectangular pattern (dimensions of 3-5 mm by 20-30 mm) having a density of scanning lines near to 7000 lines/inch. Different scan speeds and percentages of beam overlap rendered laser average travel speeds of up to a 3.3 mm/s. A maximum laser power of up to 240 W was used to melt the 2 mm thick loose powder bed. The resulting solidified ingots were separated into categories based on their surface homogeneity and shape integrity.

Metallographic analysis at low and high magnification by means of optical microscopy and scanning electron microscopy was performed on the cross section and longitudinal section of the ingots showing best surface and shape integrity. The specimens were hot mounted in transparent resin and then grinded and polished with fine alumina solution and etched with potassium bi-chromate solution. Oxygen and chlorine contamination were simultaneously measured by EDS. Vickers micro hardness was measured along the longitudinal and cross sections using a 100 grams load and a 15 sec indentation time. A total of 6 measurements were done along the width of the ingot for each specimen. Density of the ingot specimens was measured by arquimedes principle.

RESULTS AND ANALYSES

SLM specimens

Macro images (Figures 2-4) show three of the best as-obtained SLM copper specimen ingots and one specimen showing a multiple ripples pattern. It is observed in all first three specimens that a uniform and continuous cast half-cylindrical morphology has been obtained from the precursor Cu powder. By making the scanning pattern narrower and longer and decreasing the percentage of beam overlap ϕ (defined elsewhere [8]) the travel velocity is therefore increased and the cast height is lowered as seen in specimen A. Specimens B and C were produced both with parameters of 240 W in both cases and 1,3 mm/s and 1,4 mm/s in average travel speed respectively (v* are interpolated values) and a 23% variation in percentage beam overlap. Specimen C shows a short-length flow instability at the beginning of the cast that could be attributed to the slight change in speed. In the case of specimen D (Figure 5), a total of 7 flow instabilities (ripples) formed when the laser power was reduced from 240 to 200 W, the average laser travel speed reduced from 3.33 mm/s to 1.2 mm/s and the width of the rectangular pattern increased by a 50%, keeping the same percentage of beam overlap, ϕ = 15.6%.

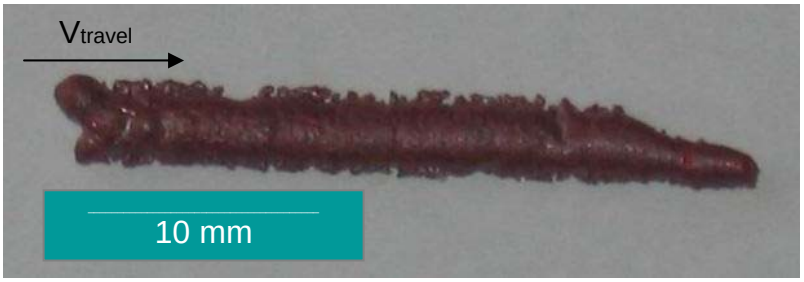

Specimen A :
Length 30 mm
Width 2.2 mm
SS 360, SP 27
Δx 0.0002 inch
Δy 0.01 inch
240 W, v = 3.3 mm/s
ϕ=15.6 % overlap

Figure 2. Showing a homogenous surface that sharpens at the end of the process. High amount of sintered particles are attached laterally.

Specimen B :
Length 18 mm
Width 3.0 mm
SS 625, SP 27
Δx 0.000125 inch
Δy 0.015 inch
240 W, v*= 1.3 mm/s
ϕ=23.5 % overlap

Figure 3. Showing a homogenous surface with good integrity.

Specimen C :
Length 19 mm
Width 3.5 mm
SS 600, SP 27
Δx 0.000125 inch
Δy 0.015 inch
240 W, v* = 1.4 mm/s
ϕ=19 % overlap

Figure 4. Showing single flow instability at the beginning of the laser melting stage that created two fronts that merged into one.

Specimen D
Length 30 mm
Width 8-4 mm
SS 360, SP 27
Δx 0.0002 inch
Δy 0.015 inch
200 W, v = 1.2 mm/s
ϕ=15.6 % overlap

Figure 5. Showing one multiple flow instabilities along the laser melting stage. A total of 7 ripple lines have resulted after solidification.

Optical microscopy analysis

Columnar grains parallel to the longitudinal or laser travel direction have been revealed by low magnification optical microscopy (Figures 6-9), the cross section observations confirm this orientation and further indicate the grains are 10 to 100 μm in diameter and almost equiaxed, with increasing diameter towards the surface of the cast material.

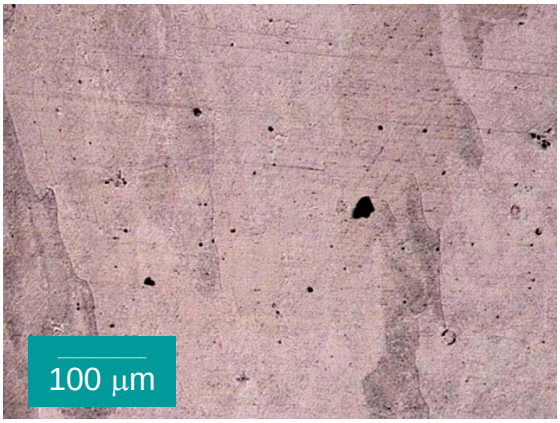

Figure 6. Optical micrograph of the longitudinal section of specimen B, x100. Showing elongated columnar grains parallel to the laser traveling direction.

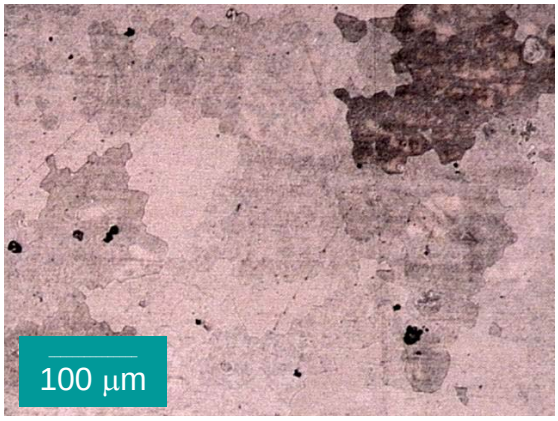

Figure 7. Optical micrograph of the cross section of specimen B, x100. Showing 100 μm size columnar grains growing parallel to the laser traveling direction.

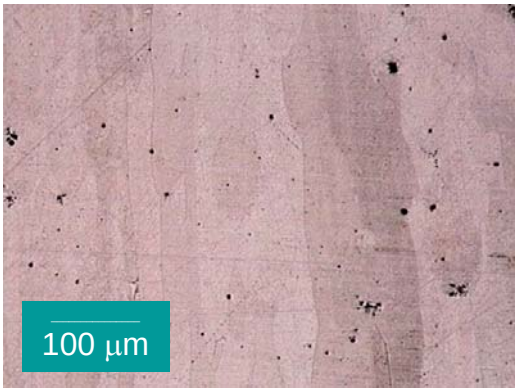

Figure 8. Optical micrograph of the longitudinal section of specimen C, x100. Showing elongated columnar grains parallel to the laser traveling direction.

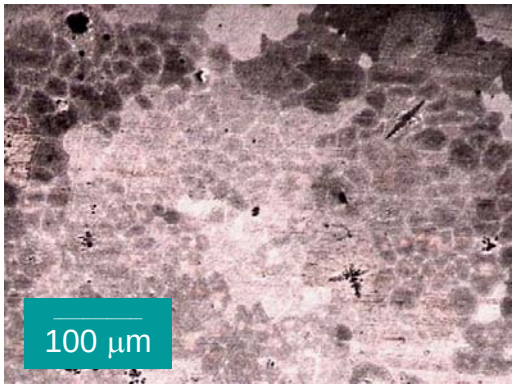

Figure 9. Optical micrograph of the cross section of specimen C, x100. Showing 10 μm size columnar grains growing parallel to the laser traveling direction.

High magnification optical microscopy (Figures 10-13) shows that almost continuous solidified structure was achieved. Inside the columnar grains a fine eutectic structure is also present. Figure 11 shows a fine dendritic structure parallel to the laser

travel direction. Surprisingly, some dendrites appear at random positions with secondary arms in direction perpendicular to the longitudinal direction in both specimens B and C. A fine dispersion of dark particles in the copper matrix suggest that a eutectic microstructure has formed containing CuO or metastable Cu_2O particles as the second phase as it will be suggested by the oxygen content presence indicated later and the Cu-O equilibrium phase diagram [9].

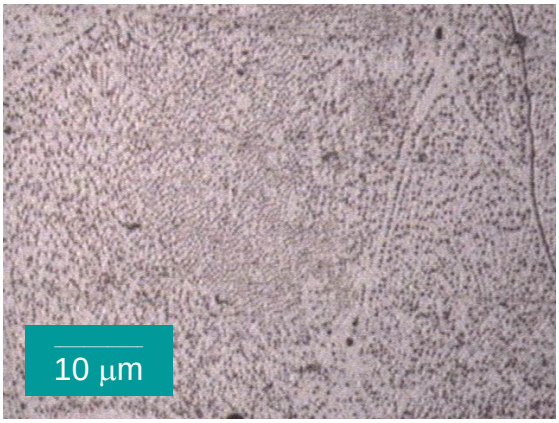

Figure 10. Optical micrograph of the longitudinal section, of specimen B, x1000. Showing a fine eutectic structure inside a grain region.

Figure 11. Optical micrograph of the cross section of specimen B, x1000. Showing a fine eutectic structure surrounding a relatively large dendrite inside a grain region.

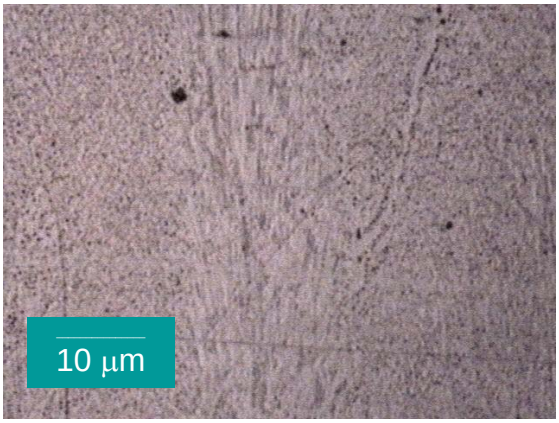

Figure 12. Optical micrograph of the longitudinal section of specimen C, x1000. Showing at the center a fine dendritic structure inside a grain region with a clear alignment direction.

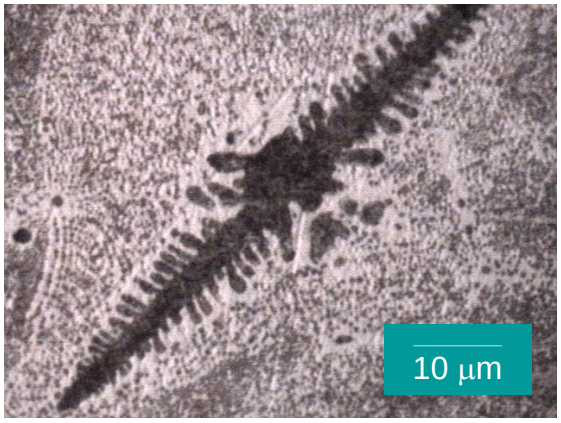

Figure 13. Optical micrograph of the cross section of specimen C, x1000. Showing a fine eutectic surrounding a large dendrite with secondary and tertiary arms developed.

Variable pressure SEM analysis

In Figure 14 and 15, high magnification VPSEM obtained with secondary electrons reveals that specimen A and B have a large presence of submicron size pores. In Figure 14 also a fine eutectic structure can be distinguished. On the other hand Figure 16, reveals that low porosity has resulted in specimen C, indicating that melting of the Cu powder was the principal forming mechanism that took place together with liquid phase sintering instead of pure sintering mechanism.

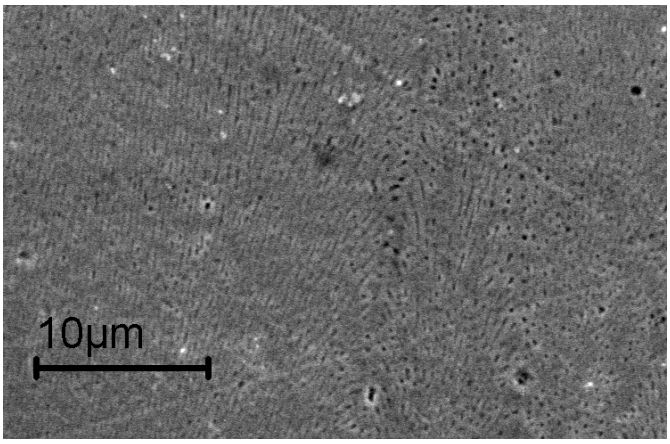

Figure 14. Variable pressure SEM SE image of the longitudinal section of specimen A, 5000x. Several submicron size pores are observed all over the region indicating that the solidification structure achieved is not 100% dense. A fine dentritic structure is also observed with a direction almost parallel to the laser traveling direction.

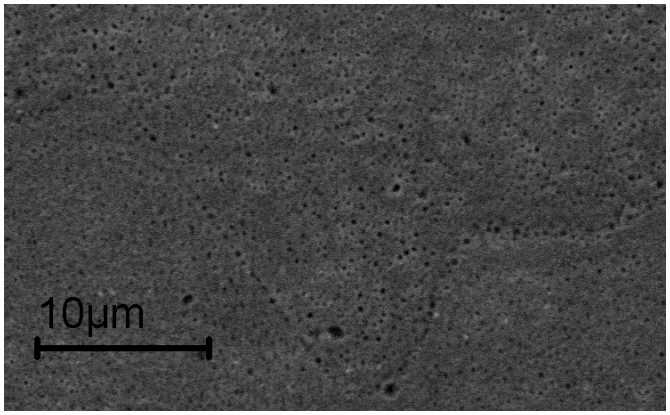

Figure 15. Variable pressure SEM SE image of longitudinal section of specimen B, 5000x. Several submicron size pores are observed all over the region indicating that the solidification structured achieved is not 100% dense. Pores are also present along grain boundaries signaling in this case a possible weak intergranular bonding.

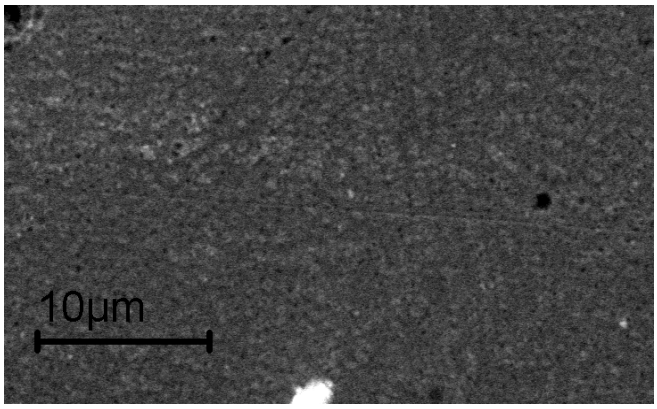

Figure 16. Variable pressure SEM SE image of longitudinal section of specimen C, 5000x. Only one micron size pore is seen, indicating in this case that the solidification structure achieved is near to 100% dense.

EDS and Vickers microhardness analysis

The semi quantitative analysis shown in Table 1 indicates that elemental oxygen was the principal contaminant from a 5.5 at% up to 8.1 at%. A source for this contaminant comes from the Cu powder which was not degassed sufficiently before the SLM process was done. Specimen C additionally showed the presence of chlorine atoms up to a 0.91 at % as showing in Figure 17. It is not known the source of this latter element. The elemental mapping distribution shown in Figure 18a-c indicates that the oxygen and chlorine contaminants are distributed homogeneously through out the Cu matrix. Oxygen is then thought to be present in the form of a fine eutectic second phase of CuO or metastable Cu_2O.

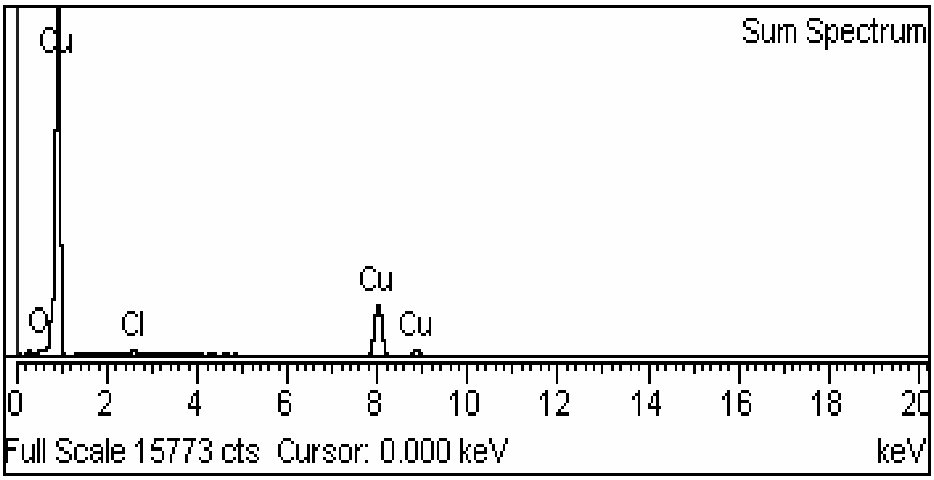

Figure 17. Energy Dispersive Spectrograph of specimen C indicating presence of oxygen as well as a minor presence of chlorine.

The microhardness values along the longitudinal section for specimen A and B differ only by a 2% difference, whereas for specimen C it shows a 8 % reduction in the HV value compared to specimen A. Values measured from the cross section of specimens B and C show a slight increase in the HV values, but similar trends. The latter specimen has a grain diameter size smaller by almost ten times compared to specimen B, however that grain size different has not meant a higher HV value. It is worth mentioning that all these HV values correspond to a 20% to 25% cold rolled oxygen free copper material (80-90 HV) [10]. Density measured by arquimedes principle gives values that are under those of pure copper.

TABLE 1: semi quantitative elemental composition of the SLM specimens, their average Vickers microhardness along the longitudinal and cross section sections and density

Specimen	% at Cu	% at O	% at Cl	Hardness Vickers Longitudinal	Hardness Vickers Cross section	Density kg/m^3
A	**91.9**	**8.1**	**-**	**90.3**	**-**	**7355+/-1218**
B	**94.5**	**5.5**	**-**	**88.4**	**89.9**	**6211+/-831**
C	**93.2**	**5.8**	**0.9**	**83.9**	**85.2**	**7125+/-1141**

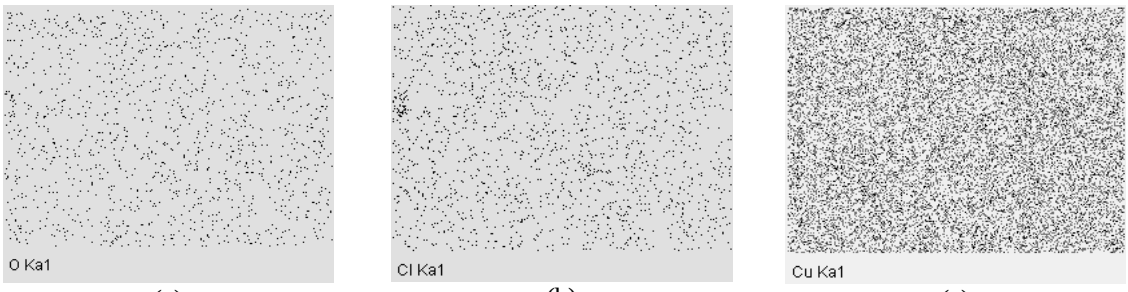

(a) (b) (c)

Figure 18.EDS elemental mapping of O, Cl and Cu in specimen C along the longitudinal section

CONCLUSIONS

Selective laser melting of fine Cu powder allows building cast structures from a single laser scanning pass at a laser power of 240 W and travel speeds in the range of 1.3 mm/s to 3.3 mm/s.

Bulks having good integrity have been cast showing a columnar grain structure aligned to the travel direction of the laser melting front. This observation also suggests that the heat flow from the melting front is parallel to this travel direction. The obtained HV values correspond to a 20% to 25 % cold rolled oxygen free copper. These values could be related to the small cross section size of the columnar grains.

Oxygen contamination could also be another reason for the increase in the microhardness value as the microstructure of the ingot is that of a fine eutectic consisting of copper and it oxides (CuO and Cu_2O). Oxygen contamination could be reduced by performing a high temperature high vacuum degassing cycle previous to the SLM process.

The ingots thus produced suggest that a multilayer structure from Cu powder could be build effectively by the SLM process having sufficiently adequate compositional, microstructure and mechanical properties for functional applications.

Future work will be focused in correlating the process parameters used with the morphology achieved (flow instability see Figure 5) in order to find a theoretical explanation for the behavior observed. The Rayleigh instability phenomenon [11] which is driven by inertia and constrained by surface tension on the liquid volume previous to solidification may provide an answer to these observations.

REFERENCES

1. J.J.Beaman, J.W.Barlow, D.L.Bourell, and R.H.Crawford, Solid Freeform Fabrication: A New Direction in Manufacturing, (Kluwer Academic, 1997).
2. 3. L. Lü, J. Fuh and Y.S. Wong, Laser Induced Materials and Processes for Rapid Prototyping, (Kluwer Academic, 2001).
3. A. Simchi, F. Petzoldt, H. Pohl, "On the development of direct metal laser sintering for rapid tooling", J.Mat. Proc.Tech., 141, (2003) 319-328.
4. R. Morgan, C.J. Sutcliffe, W.O. Oneill, "Density analysis of direct metal laser re-melted 316L stainless steel cubic primitives" Journal of Materials Science 39 2004 1195-1205.
5. H.H. Zhu, L.Lu, J.Y.H. Fuh, "Development and characterization of direct laser sintering Cu-based metal powder", J.Mat. Proc. Tech., 140 (2003) 314-317.
6. H. Kyogoku, J.A. Ramos, D.L. Bourell "Laser Melting of Ti-Ni Shape Memory Alloy" SFF Symposium 14, (2003) 668-675.
7. S. Das *et al.*, "Direct laser fabrication of a gas turbine engine component – microstructure and properties – part I", *SFF Symposium Proc,* 10, 1-9 (1998).
8. Ramos J., Bourell D.L., (2003) Mechanics of Laser Raster Scanning. Proceedings of the 14th Solid Freeform Fabrication Symposium, Austin, Texas. 559-572.
9. M. Hansen, Constitution of Binary Alloys, 2nd Ed., McGraw Hill, 1958.
10. Copper Development Association UK, http://www.cda.org.uk
11. G. Lock, Latent Heat Transfer, Oxford University Press, 1996.